An optically-based inverse method to measure in-plane permeability fields of fibrous reinforcements

Sébastien Comas-Cardona, Benoît Cosson, Simon Bickerton, Christophe Binetruy

An optically-based inverse method to measure in-plane permeability fields of fibrous reinforcements

S. Comas-Cardona [a,b,*], B. Cosson [b], S. Bickerton [c], C. Binetruy [a,b]

[a] Research Institute in Civil Engineering and Mechanics (GeM), UMR CNRS 6183, Centrale Nantes, 1 rue de la Noë, 44321 Nantes, France
[b] Department of Polymers and Composites Technology & Mechanical Engineering, Mines Douai, 941 rue Charles Bourseul, 59508 Douai, France
[c] Centre for Advanced Composite Materials, Department of Mechanical Engineering, The University of Auckland, Private Bag 92019, Auckland, New Zealand

Structural composite manufacturing relying on Liquid Composite Molding technologies is strongly affected by local variability of the fibrous reinforcement. Optical techniques using light transmission are used and allow field measurements of areal weight (and fibre volume fraction) of glass fibre reinforce-ment. The coupling of obtained areal weight mappings along with injection flow fronts is used to extract in-plane permeability fields. The current work presents results with a focus on glass random mats, but the method can be adapted to any glass fibrous medium. A study of convergence and error due to discret-ization is performed. Also the influence of the stacking of fibrous layers on the preform variability is ana-lyzed. The major advantage of the proposed technique is a relatively fast acquisition of statistical data on reinforcement variability, which can be later utilized in stochastic based process simulations.

Keywords: Fabrics/textiles, Rheological properties, Transport properties, Resin transfer molding (RTM)

1. Introduction

The manufacturing of fibre-reinforced structural composites is influenced by the variability of the constituent materials (i.e. fibrous media and organic matrix). Processing methods involving significant resin flow through the fibre reinforcement, for example the Liquid Composite Moulding techniques, are strongly affected by variability in the reinforcement structure. For a given fibrous reinforcement, local variations in fibre content and orientation exist [6] and will lead to variation in permeability and through-thickness compaction response. Significant in-plane variability has been shown to exist within a single reinforcement layer, and the influence of this variability can possibly be modified as multiple-layer preforms are assembled [1–5,8,10,13]. A new field of research has emerged with respect to modeling the variability of composite manufacturing, especially during the injection stage [11,15,17,21]. Stochastic simulation can help quantifying the robustness of a process, which is of major importance for high series production such as in the automotive industry.

In a deterministic numerical formulation, the resin injection stage is modeled coupling Darcy's law with the conservation of mass. The inputs for such models are the resin viscosity, the fibrous medium permeability tensor, the domain geometry and initial and boundary conditions. The input being unique will lead to a unique (deterministic) solution. However, when stochastic manufacturing simulations are performed, the inputs must represent some extent of variability in the process and/or materials. For instance in the case of Resin Transfer Molding (RTM) one can agree that the mold geometry is not too variable whereas the permeability can be highly dispersed from preform to preform and even within the preform itself. Therefore when stochastic simulation is of concern, the input cannot be a unique value, but has to be a field (in space and/or in time). The new challenge is to propose techniques that can provide the field of the variable parameters required in the stochastic simulations. For example, a previous study coupling optical techniques with numerical flow simulation have been proposed [9].

This paper focuses on measuring the in-plane permeability field of single- or multi-layers of fibrous reinforcement. The technique has been developed around the measurement of the areal weight field of each layers coupled to central injection of the samples. It is an alternative to the statistical technique based on image analysis of dry fabrics and permeability models proposed in [22]. Recorded injection pressure and flow front data are utilized with a finite element/level set based inverse method, which solves for the unknown in-plane permeability field.

It is worth mentioning that both porosity and permeability are parameters that depend on the volume where averaging is performed. The results in [22] have shown that, for the material of interest in this study, a 95% confidence on porosity and permeability values is attained for respectively 10 and 350 mm square-sample size. Here because of the discretization, which will be modified

* Corresponding author at: Research Institute in Civil Engineering and Mechanics (GeM), UMR CNRS 6183, Centrale Nantes, 1 rue de la Noë, 44321 Nantes, France.
E-mail address: sebastien.comas@ec-nantes.fr (S. Comas-Cardona).

along the study, the porosity and permeability fields presented are apparent values. For the sake of simplicity, the adjective apparent will not be used in the following when referring to either porosity or permeability.

First, the setups for areal weight field measurement and central injection flow fronts are briefly described. Then, the methodology based on an inverse method is detailed. Finally results of permeability fields are given. The sensitivity of the results with respect to the number of stacked layers and numerical discretization is discussed.

2. Experimental setups for field-measurements

2.1. Materials

The fibrous material is an E-glass chopped strand mat (CSM) whose reference is M705450 (Owens Corning). It has an average areal weight of 457 (+/-24) g/m^2 measured on 37 samples. The fibrous material has been statistically studied for average and local porosity and permeability fields in a former study [22]. The mineral oil used in the central injection has a viscosity of 0.21 Pa s at room temperature. Because of possible temperature variation from one test to another, the temperature was recorded for each injection, then the viscosity was interpolated from a viscosity measurement database. Also one injection lasted around 1 min, therefore the risk of significant temperature change during the injection is negligible.

Since CSM are made of thin tows, the local unsaturation induced by the dual-scale porosity is very limited; there is no need to develop a multi-scale FE model to solve for fluid flow to get the intrinsic (also referred as effective or saturated) permeability [16]. Then the permeability field identified through the proposed technique is assumed to be a mapping of Darcian permeabilities. For woven or fibrous materials that would consist of large tows (therefore presenting a double scale porosity), another model including that feature should be used.

2.2. Areal weight measurements

An apparatus consisting of a light-box and digital SLR camera is used to capture high-resolution images of the reinforcement layers [6]. By characterizing the relationship between intensity of the transmitted light through the reinforcement and the corresponding areal weight, image analysis techniques have been developed and are capable of translating the surface images into maps detailing areal weight spatially. Optical distortions such as vignetting and barrelling have been compensated for within these analyses. Also the effect of non-homogenous back lighting has been eliminated. Readers can refer to the work carried out by Gan et al. for the details of the technique [6].

2.3. Injection and flow front measurements

Central injections at constant pressure (0.1 MPa, 1 bar) are realized within a cavity consisting of a bottom glass platen and top cylindrical aluminum platen. The mineral oil is used as a model Newtonian fluid. The 25 cm $\times$ 25cm fibrous reinforcement preform is positioned in the mold cavity. The plies have been punched with a 15 mm-diameter hole to create a circular injection inlet at the centre of the sample. In order to avoid risks of variability of the holes' diameters and ensure a clean cut, the latter are very efficiently and reproductively punched with a hydraulic press.

The injection setup is mounted in an Instron universal testing machine (Fig. 1). The cavity thickness is set from the total areal weight of the single or stacked plies to achieve a target fibre

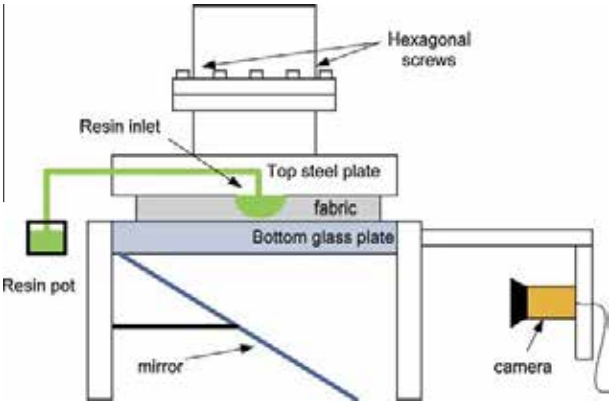

Fig. 1. Experimental injection setup [20]. (For interpretation of the references to color in this figure legend, the reader is referred to the web version of this article.)

volume fraction V_f of 38%. A CCD camera records the flow front progression with time through the transparent glass platen (Fig. 2). The digital images are processed so as to extract flow front profiles (Fig. 3 (bottom). The flow front profiles can also be plotted in radial coordinates (r, θ (where $x = r\cos\theta$ and $y = r\sin\theta$) to better visualize front distortions and variability with respect to space and time (Fig. 3 (top left)) [14]. As expected at constant injection pressure, the flow front slows down with respect to time (the fronts are not equidistant for a given time step). In order to even better visualize the extent of distortion without being penalized by that effect, the fronts can also be plotted in a (r^2, θ space that forces the injection fronts to be more equidistant (Fig. 3 (top right)). In other words, in the (r^2, θ space, a slowdown or rise of the flow front speed due to local permeability change can be more easily observed independently from the inevitable slowdown induced by the central injection at constant inlet pressure.

3. Data processing methodology

3.1. Fibre volume fraction

With a cavity thickness t in which the reinforcement is applied, areal weight fields obtained from the image analysis mentioned earlier are converted to fibre volume fraction fields using:

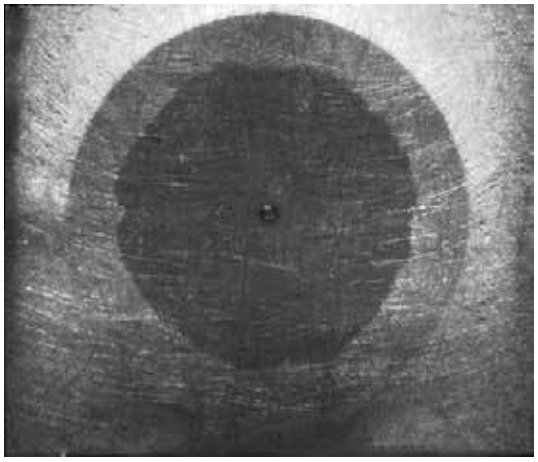

Fig. 2. Raw image taken through the bottom glass platen during the central injection of a chopped strand mat (CSM) material after 54 s of injection. The fibrous CSM appears in light gray, the circle (in intermediate gray) is the top platen and the darkest area is the impregnated material.

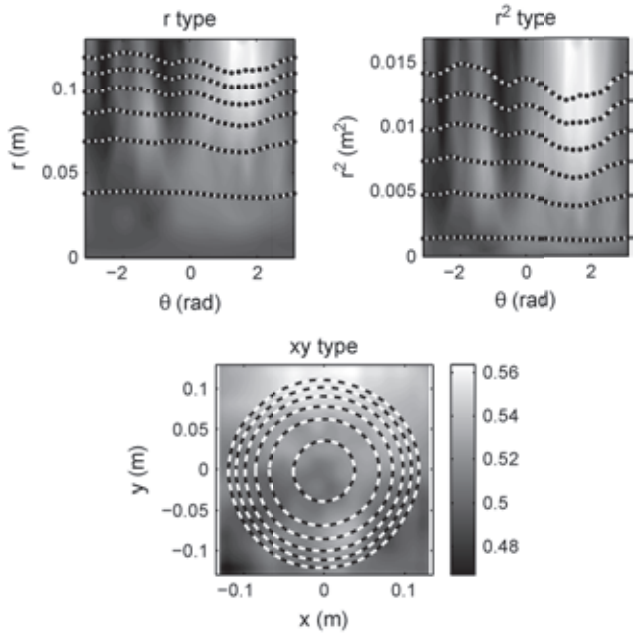

Fig. 3. Superposition of fabric porosity (background) and experimental flow front positions at various times (dashed lines). One set of results obtained from one experiment are plotted in (x, y) coordinates (bottom), in radial (r, θ coordinates (top left) and in (r^2, θ coordinates (top right).

$$V_f = \frac{\sum_{i=1}^{N} A_w^i}{t\rho_f} = 1 - \phi \tag{1}$$

where A_w^i is the reinforcement areal weight of the ith ply, N is the number of plies in the considered stack, ϕ the porosity and ρ_f is the density of the glass fibres. From the corresponding volume fraction fields, it was observed that the data varied by up to +/-10% as a function of (x, y) location, having no structured or predictable distribution spatially (Fig. 4). These intrinsic variations in fibre volume fraction are a result of the differences in the local fibre architecture introduced during reinforcement manufacturing.

3.2. From flow fronts to permeability field

As shown in the previous section, the fibre volume fraction (or porosity) of the fibrous sample is not constant in space. As a consequence of this variability, the permeability of fabrics will also be a function of space. In this section, an original method is proposed to identify the permeability field of fabrics using an inverse method.

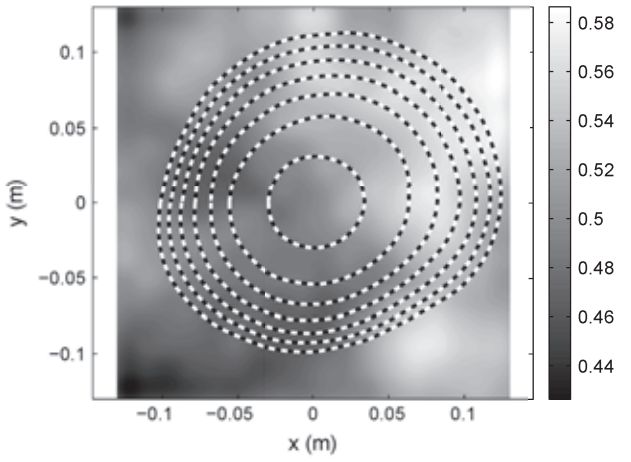

Fig. 4. Example of flow front positions (black broken lines) extracted from experimental injections and porosity (greyscale background) obtained from light-box analysis in (x, y) coordinates for 1 ply.

First numerical flow fronts have to be calculated numerically. Because flow fronts are moving boundaries driven by fluid flow dynamics, the numerical method combines the finite element (FEM) and the level set methods. The level set method is used in a variety of applications (chemical or fluid simulations [7,12,18,21]). The goal of this method is to track a moving boundary within a simulated two-phase flow without re-meshing the domain where the FEM is used. The flow front Γ is defined as:

$$\Gamma(t) = \{x \in R^2 : \psi(x, t) = 0\} \tag{2}$$

with

$$\psi(x, t) = \pm \min \|x - x_\Gamma\| \tag{3}$$

where ψ is the level set function. The level set function is the signed distance function: it is the distance between a point and the front. In the case of porous medium flow simulations (described by Darcy's law), the two moving phases are the injected resin and the air expulsed ahead of the front. The level set function is negative within the resin domain, equal to zero at the flow front location and positive outside the resin domain (i.e. in the air domain) (Fig. 5). This method has already been used previously for LCM simulations [18,21].The evolution of the flow front position is then described by the following evolution equation, which is given in [19].

$$\frac{\partial \psi(x, t)}{\partial t} + v(x, t) \cdot \nabla \psi(x, t) = 0 \tag{4}$$

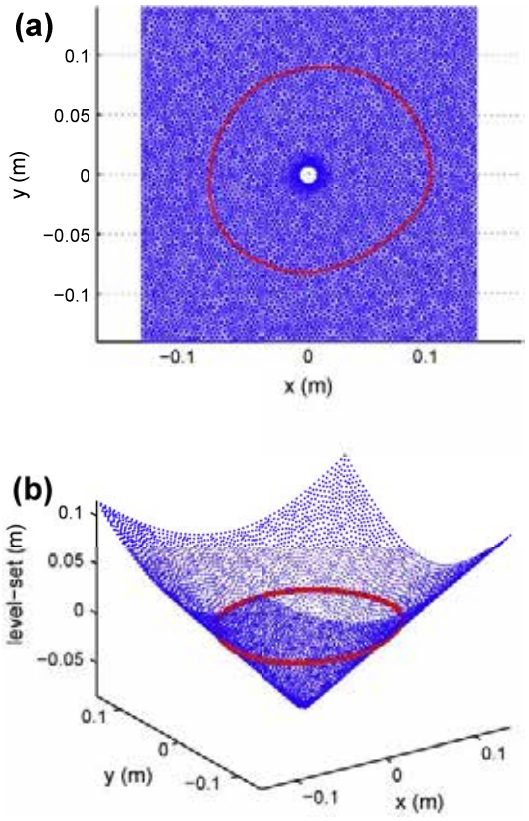

Fig. 5. Level set representations. (a): Superposition of finite element mesh (background), and level set function which delimits the flow front position Γ (solid line). (b): Level set function ψ. (For interpretation of the references to color in this figure legend, the reader is referred to the web version of this article.)

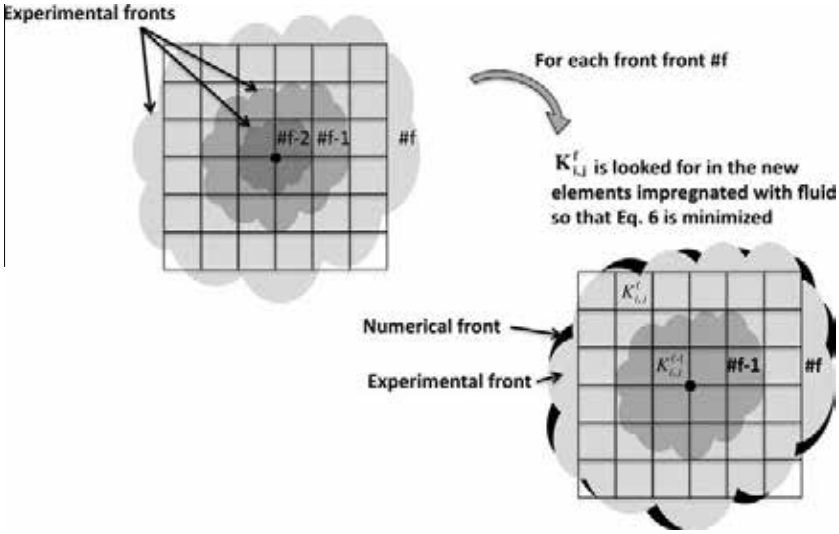

Fig. 6. Sketch of the optimization procedure.

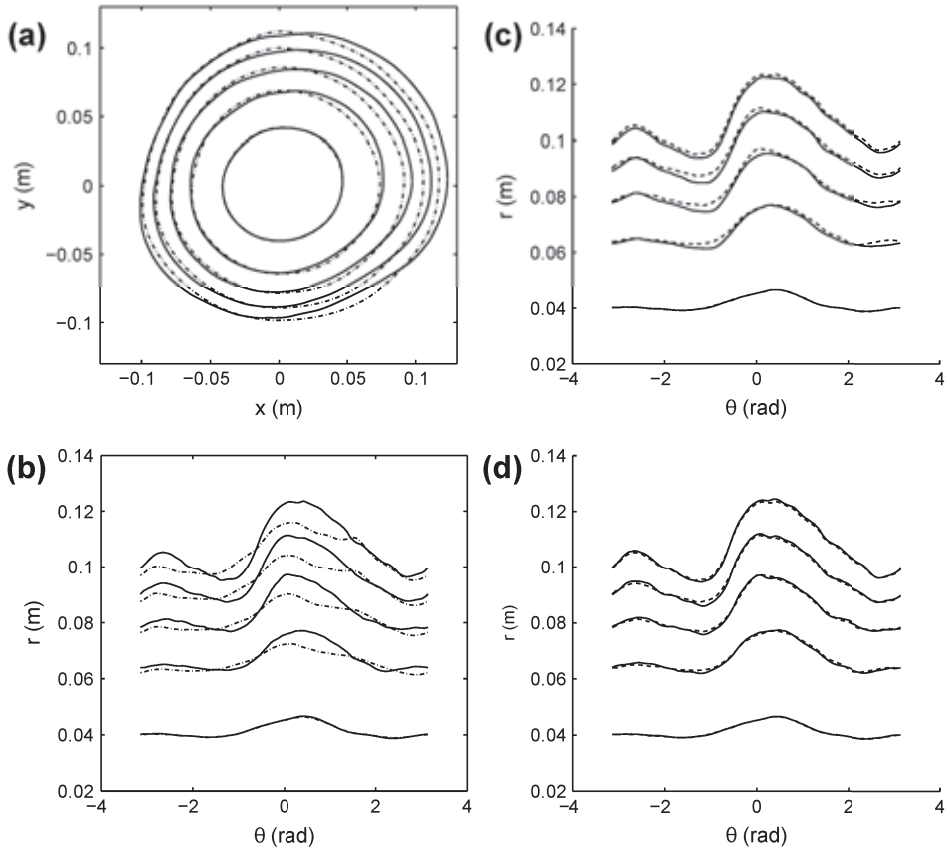

Fig. 7. Superposition of experimental (broken lines) and numerical (solid lines) flow fronts in the (x, y) or $(r, \theta$ coordinates. (a): Optimization based on 2 fronts (Error 4.1%) for the optimization based on Eq. (8) plotted in (x, y) coordinates. (b): Optimization based on 2 fronts (Error 4.1%) for the optimization based on Eq. (8) plotted in (r, θ) coordinates. (c): Optimization based on a 12×12 grid and 3 fronts (Error 1.51%). (d): Optimization based on a 24×24 grid and 5 fronts (Error 0.68%).

where $v(x, t)$ is the interstitial (observable) fluid velocity field (computed in all domains: air and resin). That function has to be reconstructed to avoid self-degradation. That reconstruction is realized calculating the true shortest distance of each element from the flow front position ($\psi(x, t) = 0$).

The velocity field is computed by solving the following set of equations (conservation of mass, Darcy's velocity definition and Darcy's law):

$$\begin{cases} \nabla \cdot (\phi(x) v(x,t)) = 0 \\ v(x,t) = \frac{u(x,t)}{\phi(x)} \\ u(x,t) = -\frac{K(x)}{\mu} \nabla p(x,t) \end{cases} \quad (5)$$

where $p(x, t)$ is the pressure field, $u(x, t)$ is the Darcy's velocity field, $K(x)$ is the permeability field, μ is the viscosity (close to 0.21 Pa s when x is in the resin domain and $\mu = \mu_{air} = \alpha\mu_{resin}$ when x is in

Table 1
Inverse method residual error when various grid sizes and number of fronts are considered in the optimization.

	Number of fronts	Grid size	Error E (Eq. (6)) (%)
Influence of grid size	3	12×12	1.51
	3	20×20	1.44
	5	20×20	0.79
	5	24×24	0.68
Influence of number of fronts	3	20×20	1.44
	4	20×20	1.09
	5	20×20	0.79

Table 2
Error evolution with respect to number of plies constituting the preform.

Number of plies	Number of fronts	Grid size	Error E (Eq. (6)) (%)
1	4	20×20	1.09
2	4	20×20	0.58
4	4	20×20	0.91
8	4	20×20	0.58

the air domain) and $\phi(x)$ is the porosity field. Great care should be taken in order to verify the convergence of the results with respect to the viscosity ratio α that can lead to numerical issues when that coefficient is chosen below 10^{-4}.

In order to identify the permeability field $K(x)$, the domain is discretised on a $n \times n$ grid. The basic concept of the inverse method is to use a minimum of flow front information in order to find the permeability field $K(x)$ which allows numerical and experimental flow fronts to match. The methodology is illustrated in Fig. 6. For a given flow front #f, the permeability field is looked for in the newly impregnated elements (between the flow fronts #f − 1 and #f), minimizing the error E (Eq. (6)) between numerical and experimental flow fronts. A Matlab code has been written and uses the predefined function *fmincon*).

$$E(\#\mathrm{f}) = \sqrt{\frac{\int_0^{2\pi} (r_{num}(\theta) - r_{exp}(\theta))^2 \mathrm{d}\theta}{\int_0^{2\pi} r_{exp}(\theta)^2 \mathrm{d}\theta}} \tag{6}$$

where r_{num} and r_{exp} are respectively the numerical and experimental flow front radial positions. The number of intermediate flow fronts used in the inverse method will be studied (ranging from 3 to 5 fronts).

In order to estimate an overall error over the entire sample domain, another cumulative error is calculated:

$$E_r(\#\mathrm{f}) = \sqrt{\frac{\int_0^{t_f} \int_0^{2\pi} (r_{num}(t,\theta) - r_{exp}(t,\theta))^2 \mathrm{d}\theta \mathrm{d}t}{\int_0^{t_f} \int_0^{2\pi} (r_{exp}(t,\theta))^2 \mathrm{d}\theta \mathrm{d}t}} \tag{7}$$

where t_f is the final injection time. That error is used as an estimation of the overall "quality" of the optimizations realized over the entire sample.

The sought $n \times n$ permeability field can be a large matrix. First, in order to limit the number of degrees of freedom, the permeability field is calculated from the porosity field (Fig. 4). It is established that, at the first order, the permeability is directly linked to the porosity (or fibre volume fraction). In Zhang et al. [22] it has been shown that the Kozeny–Carman relationship cannot fit the local fluctuations of the chopped strand mat reinforcement whose fibrous clustering is quite relevant. Because the Kozeny–Carman relationship has only one adjustable parameter (the Kozeny constant), in this study, the choice is made to use a permeability law containing two coefficients. Therefore, at first, the calculation of the permeability field is performed with an estimator based on a power law:

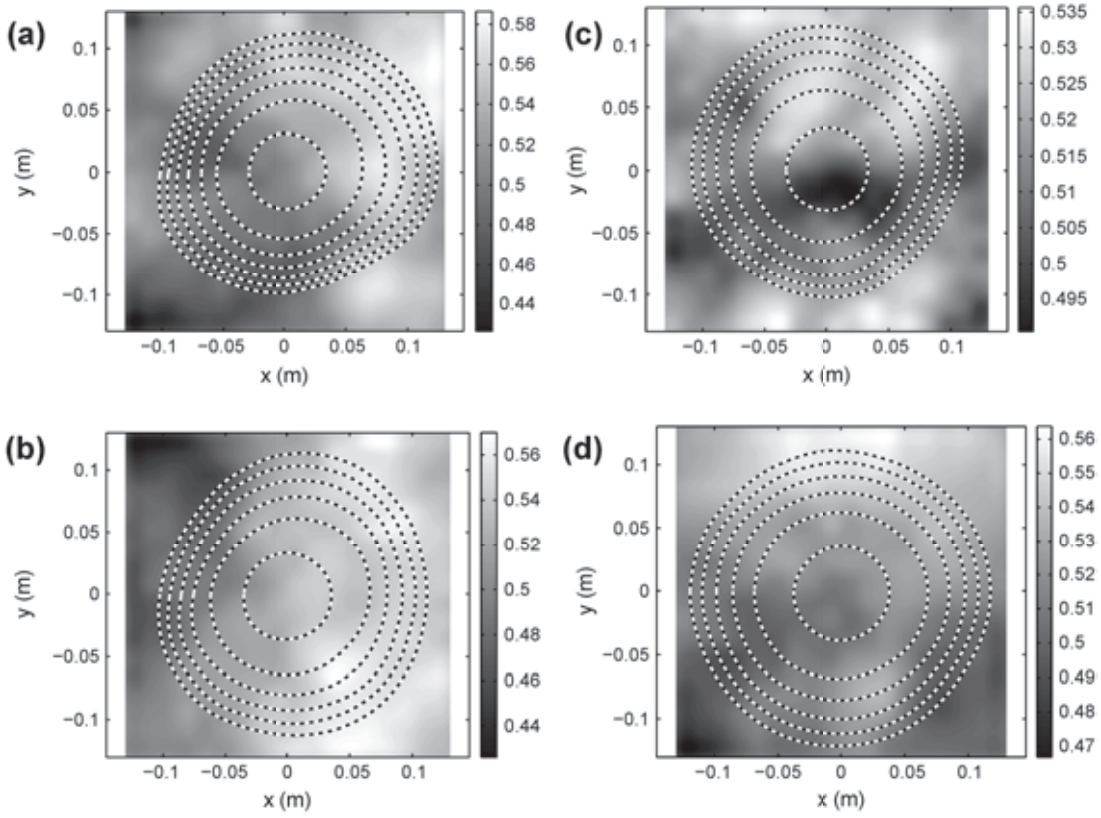

Fig. 8. Superposition of experimental flow fronts (broken lines) and porosity (background) plotted in the (x, y) coordinates. (a): 1 ply. (b): 2 plies. (c): 4 plies. (d): 8 plies.

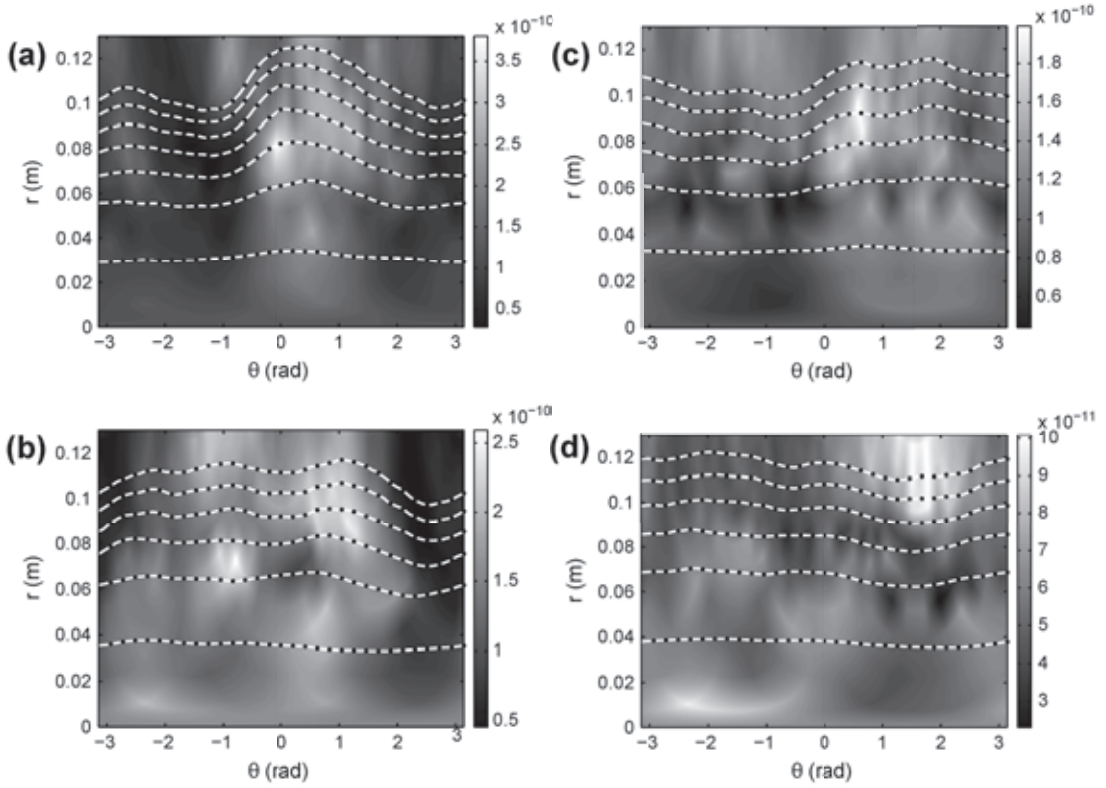

Fig. 9. Superposition of experimental flow fronts (broken lines) and permeabilities (background) plotted in the (r, θ coordinates. (a): 1 ply. (b): 2 plies. (c): 4 plies. (d): 8 plies.

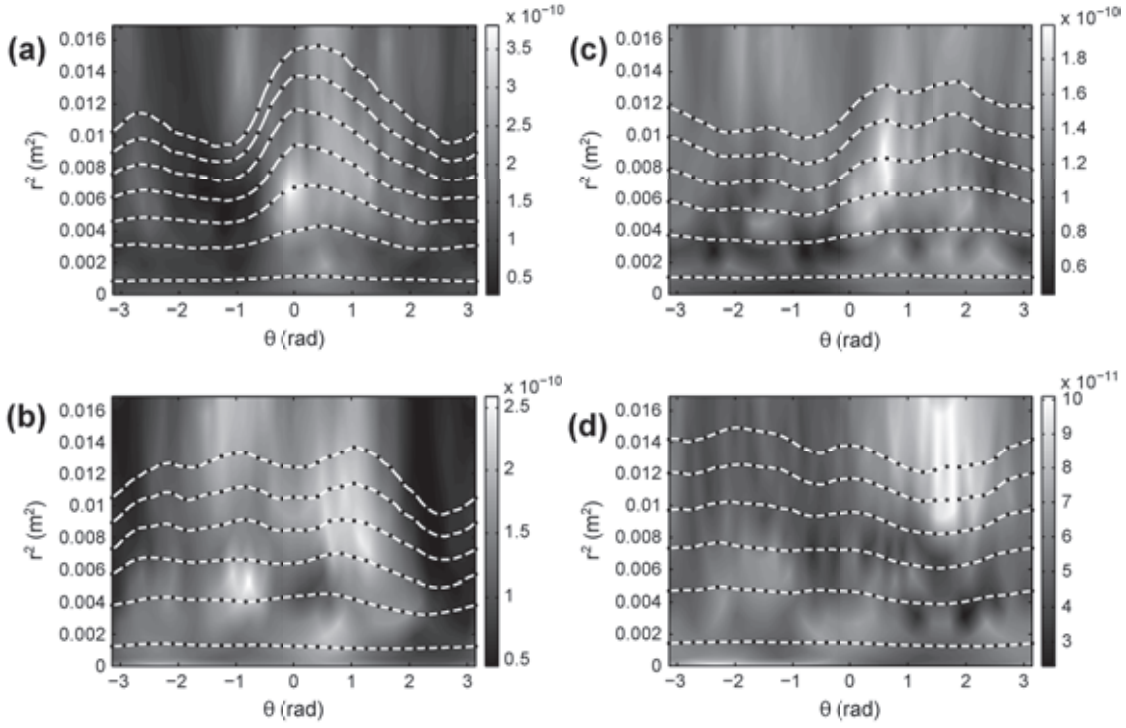

Fig. 10. Superposition of experimental flow fronts (broken lines) and permeabilities (background) plotted in the (r^2, θ coordinates. (a): 1 ply. (b): 2 plies. (c): 4 plies. (d): 8 plies.

$$K(x) = A[\phi(x)]^B \tag{8}$$

This choice also has an advantage of looking for only two scalar parameters (A, B) for the whole permeability field extraction that would minimize Eq. (6).

In a second study and in order to increase the accuracy of the technique, the entire permeability field is looked for individually, i.e., $n \times n$ independent values are sought. Because of the size of unknowns to be found, in order to speed up the minimization of Eq. (6), the optimum (A, B) values obtained previously will be used

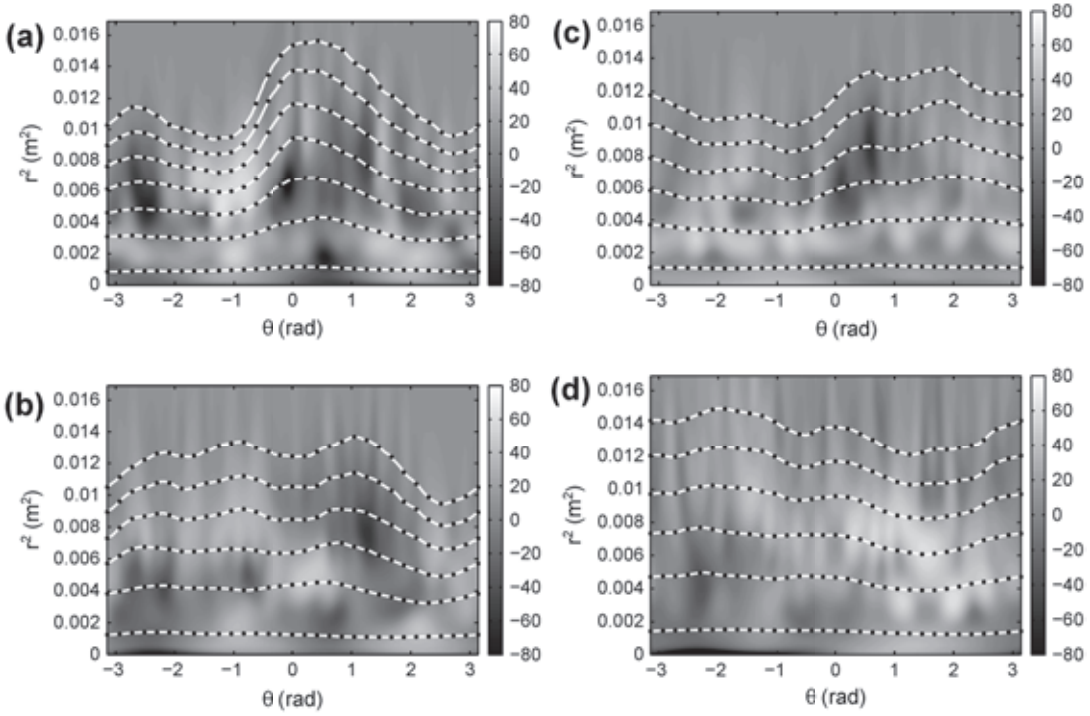

Fig. 11. Superposition of experimental flow fronts (broken lines) and permeability variation fields (in %) plotted in the (r^2, θ coordinates. (a): 1 ply. (b): 2 plies. (c): 4 plies. (d): 8 plies.

as a first guess. To achieve this goal, the optimization will be done again with the *fmincon* function in Matlab.

In order to limit the calculation time while maintaining some extent of accuracy, the optimization can be performed based on a certain number of experimental flow fronts and on coarser/finer grids. The following sections will analyze the effect of those two parameters comparing the errors given by Eq. (7). Also the evolution of the permeability variability with respect to the amount of plies stacked in the preform will be studied.

4. Results and discussion

4.1. Influence of number of degrees of freedoms

Fig. 7 shows that permeability fields can be found. However, depending on the number of degrees of freedom (2 (i.e., A and B in Eq. (8)) in Fig. 7a and b and $n \times n$ in Fig. 7c and d) the experimental and simulated flow fronts clearly match differently. The use of a first order estimator for permeability (*i.e.*, V_f) is not sufficient (Fig. 7a and b). This has been shown in a previous study based on a similar fibrous mat that used an optical device and image analysis [22]. It has been shown that local permeability is affected by clustering and relative position of V_f heterogeneities. That is why more degrees of freedom are required for a better flow front match. The remaining of the article will focus on the $n \times n$ optimization.

4.2. Influence of the discretization grid and number of flow fronts

First, the calculations to estimate the influence of both discretization grid and number of flow fronts are performed and discussed on samples of 1 ply of mat. As shown in Table 1, the permeability identification using an inverse method is realized with various numbers of fronts and grid sizes. The error (cumulative difference of experimental and simulated flow fronts (Eq. (7))) decreases when the number of flow fronts and/or grid size increases. Fig. 7(c and d) shows the corresponding experimental and numerical flow fronts plotted for permeability field calculated using respectively a 12×12 mesh grid along with 3 flow fronts and a 24×24 mesh grid along with 5 flow fronts. As expected, it clearly emphasizes that the numerical flow front matches increasingly well when finer grids along with more flow fronts are used in the procedure. Above 1% of error, the flow fronts visually do not match well, it is important to ensure an error below 1% for an acceptable match.

4.3. Influence of the number of plies in a stack

Once the grid size has been set, the methodology has been used on stack consisting of multiple layers (2, 4 and 8). The choice of plies to be stacked has been done randomly. Fig. 8(a–d) shows the experimental results in terms of flow front positions and porosity fields. As expected, it can be seen that increasing the number of plies decreases the flow front distortions and the porosity variations within the preform.This effect can also be seen in Table 2. The permeabilities are calculated following the procedure detailed in this article and are displayed in Figs. 9 and 10. They show that the homogeneity of the permeability field increases with the number of plies.

Finally, a comparison of deviation between the 2 degrees of freedom method and the $n \times n$ optimization is depicted in Fig. 11. It shows the permeability variation $(K_{num} - K_{power})/K_{num}$, where K_{power} is the local permeability solution from the power-law relationship and K_{num} is the local permeability obtained with the $n \times n$ degrees of freedom method. Fig. 11 shows again that local permeability is not only controlled by the fibre volume fraction since a substantial deviation exists. All variation scales are similar in Fig. 11 and show that with 8 layers of CSM the permeability field is more homogeneous (it exhibits less dark and light regions). It also shows that the power law relationship can give a better

estimation of local permeability when the number of plies increases.

5. Conclusion

An inverse identification method of in-plane permeability fields based on optical measurement of areal weight fields (consequently fibre volume fraction and porosity) and central injection flow front measurements has been detailed. The results shown in this article are related to a glass fibre chopped strand mat. The permeability field extraction is realized by inverse method minimizing the error of numerical and experimental flow front positions. Two optimizations with different amounts of degrees of freedom have been checked. The results show that a permeability description based on fibre volume fraction is not sufficient. A technique with more degrees of freedom has finally been chosen. The influence of the grid size has been evaluated and the variability for various stacks has been examined. The variability, as expected, decreases when more plies are layered. Moreover, two other results can be emphasized:

- with a limited number of fronts, e.g. 3 or 5, a permeability field of dimension 24×24 can be precisely extracted;
- also the level of error given by the technique has to be carefully checked. It is shown that slightly reducing the global error from 1.7% down to 0.7% has a tremendous effect on the flow front position match.

The extension of this work to an anisotropic media is straightforward as long as the fibrous media can be used in the light-box device for areal weight measurement. For non-transparent media (such as carbon) the use of another optical technique should be considered to reconstruct the microstructure (e.g., in [9]). The major advantage of the present technique is relatively fast acquisition of statistical data on reinforcement variability, which can be later utilized in stochastic based process simulations [21].

Acknowledgments

The authors wish to deeply acknowledge the funding provided by CACM-University of Auckland and Mines Douai for the visiting periods of S. Bickerton and S. Comas-Cardona which lead to this study.

References

[1] Arbter R, Beraud JM, Binetruy C, Bizet L, Bréard J, Comas-Cardona S, et al. Experimental determination of the permeability of textiles: a benchmark exercise. Composites Part A 2011;42:1157–68.
[2] Babu BZ, Pillai KM. Experimental investigation of the effect of fiber-mat architecture on the unsaturated flow in liquid composite molding. J Compos Mater 2004;38(1):57–79.
[3] Desplentere F, Lomov SV, et al. Micro-CT characterization of variability in 3D textile architecture. Compos Sci Technol 2005;65:1920–30.
[4] Diallo ML, Gauvin R, et Trochu F. Key factors affecting the permeability measurement in continuous fiber reinforcements. In: Proceedings of ICCM-11, Gold Coast, Australia, 14–18th July, 1997. p. 441–51.
[5] Endruweit A, McGregor P, Long AC, et al. Influence of the fabric architecture on the variations in experimentally determined in-plane permeability values. Compos Sci Technol 2006;66:1778–92.
[6] Gan JM, Bickerton S, Battley M. Quantifying variability within glass fiber reinforcements using an automated optical method. Composites Part A 2012;43(18):1169–76.
[7] Gantois R, Cantarel A, Cosson B, Dusserre G, Felices J-N, Schmidt F. BEM-based models to simulate the resin flow at macro and micro scales in LCM processes. Polym Compos 2013;34(8):1235–44.
[8] Golestanian H. Physical determination of permeability variation with porosity for composite preforms. Int J Ind Eng Prod Res 2007;18(4):67–73.
[9] Lomov SV, Verpoest I, Cichosz J, Hahn C, Ivanov DS, Verleye B. Meso-level textile composites simulations: open data exchange and scripting. J Compos Mater, in press.
[10] Lundström TS, Stenberg R, et al. In-plane permeability measurements: a Nordic round-robin study. Composites Part A 2000;31:29–43.
[11] Markicevic B, Heider D, Advani SG, et al. Stochastic modeling of preform heterogeneity to address dry spots formation in the VARTM process. Composites Part A 2005;36:851–8.
[12] Marchandise E, Remacle JF. A stabilized finite element method using a discontinuous level set approach for solving two phase incompressible flows. J Comput Phys 2006;219:780–800.
[13] McGrath LM, Liu Q, Parnas RS. Statistical correlations in the permeability tensor. In: Proceedings of FPCM-8, July, Douai, France; 2006.
[14] Montes N, Sanchez F. A new computational tool for liquid composite moulding process design based on configuration spaces. Composites Part A 2010;41(1):58–77.
[15] Padmanabhan SK, Pitchumani R. Stochastic modeling of nonisothermal flow during resin transfer molding. Int J Heat Mass Transfer 1999;42:3057–70.
[16] Schell JSU, Deleglise M, Binetruy C, Krawczak P, Ermanni P. Numerical prediction and experimental characterisation of meso-scale-voids in liquid composite molding. Composites Part A 2007;38:2460–70.
[17] Skordos AA, Sutcliffe MPF. Stochastic simulation of woven composites forming. Compos Sci Technol 2008;68:283–96.
[18] Soukane S, Trochu F. Application of the level set method to the simulation of resin transfer molding. Compos Sci Technol 2006;66(7–8):1067–80.
[19] Sukumar N et al. Modeling holes and inclusions by level sets in the extended finite-element method. Comput Methods Appl Mech Eng 2001;190:6183–200.
[20] Tournier L. Method for optical measure of local reinforcement permeability and infusion behavior prediction in liquid molding processes, project report, Centre for Advanced Composite Materials, University of Auckland; 2010.
[21] Zhang F, Cosson B, Comas-Cardona S, Binetruy Efficient C. Stochastic simulation approach for RTM process with random fibrous permeability. Compos Sci Technol 2011;71:1478–85.
[22] Zhang F, Comas-Cardona S, Binetruy C. Statistical modeling of in-plane permeability of non-woven random fibrous reinforcement. Compos Sci Technol 2012;72:1368–79.